

## EDGE ARTICLE

Cite this: *Chem. Sci.*, 2020, 11, 5974

All publication charges for this article have been paid for by the Royal Society of Chemistry

# ABC triblock bottlebrush copolymer-based injectable hydrogels: design, synthesis, and application to expanding the therapeutic index of cancer immunochemotherapy†

Farrukh Vohidov,<sup>‡a</sup> Lauren E. Milling,<sup>‡b</sup> Qixian Chen,<sup>id a</sup> Wenxu Zhang,<sup>a</sup> Sachin Bhagchandani,<sup>a</sup> Hung V.-T. Nguyen,<sup>a</sup> Darrell J. Irvine<sup>id \*b</sup> and Jeremiah A. Johnson<sup>id \*ab</sup>

Bottlebrush copolymers are a versatile class of macromolecular architectures with broad applications in the fields of drug delivery, self-assembly, and polymer networks. Here, the modular nature of graft-through ring-opening metathesis polymerization (ROMP) is exploited to synthesize “ABC” triblock bottlebrush copolymers (TBCs) from polylactic acid (PLA), polyethylene glycol (PEG), and poly(*N*-isopropylacrylamide) (PNIPAM) macromonomers. Due to the hydrophobicity of their PLA domains, these TBCs self-assemble in aqueous media at room temperature to yield uniform ~100 nm micelles that can encapsulate a wide range of therapeutic agents. Heating these micellar solutions above the lower critical solution temperature (LCST) of PNIPAM (~32 °C) induces the rapid formation of multi-compartment hydrogels with PLA and PNIPAM domains acting as physical crosslinks. Following the synthesis and characterization of these materials *in vitro*, TBC micelles loaded with various biologically active small molecules were investigated as injectable hydrogels for sustained drug release *in vivo*. Specifically, intratumoral administration of TBCs containing paclitaxel and resiquimod—the latter a potent Toll-like receptor (TLR) 7/8 agonist—into mice bearing subcutaneous CT26 tumors resulted in a significantly enhanced therapeutic index compared to the administration of these two drugs alone. This effect is attributed to the TBC hydrogel maintaining a high local drug concentration, thus reducing systemic immune activation and local inflammation. Collectively, this work represents, to our knowledge, the first example of thermally-responsive TBCs designed for multi-compartment hydrogel formation, establishing these materials as versatile scaffolds for self-assembly and drug delivery.

Received 7th May 2020  
Accepted 16th May 2020

DOI: 10.1039/d0sc02611e

rsc.li/chemical-science

## Introduction

Driven by advances in their synthesis, bottlebrush polymers have experienced a renaissance in recent years, with applications ranging from drug delivery and molecular imaging to self-assembly and polymer network fabrication.<sup>1–6</sup> Of the strategies for bottlebrush polymer synthesis,<sup>7–10</sup> graft-through polymerization of macromonomers (MMs) offers advantages of complete backbone functionalization and facile access to multi-block copolymers.<sup>11–13</sup> Ring-opening metathesis polymerization (ROMP) of norbornene-based MMs is perhaps the most useful method for graft-through bottlebrush polymer synthesis thanks to its

efficiency and tolerance toward a wide range of functional groups; this approach has been used to generate bottlebrush-based polymer architectures with unique self-assembly, imaging, and drug delivery capabilities.<sup>14–17</sup> Despite these advances, and given the well-established utility of triblock copolymers in self-assembly and biomedicine,<sup>18–21</sup> there are limited examples of triblock bottlebrush copolymers (TBCs).<sup>22–24</sup> For instance, Bates and coworkers prepared two-component “ABA” TBCs from polystyrene and polyethylene glycol (PEG) MMs and demonstrated their utility as Li-ion conductors.<sup>22</sup> Additionally, reports on the solution<sup>12,23,25–28</sup> and bulk<sup>29–31</sup> self-assembly of ABA, as well as three-component “ABC” TBCs, have hinted at exciting opportunities for this class of macromolecular architectures.

We reasoned that appropriately designed ABC TBCs could serve as macromolecular precursors to injectable hydrogels with advantages including ease-of-synthesis, low critical micelle concentrations (CMCs),<sup>32</sup> and precise control over their compartment domain sizes. We were inspired by the pioneering work of Tirrell and coworkers, who showed that physical hydrogels composed of linear ABC triblock protein macromers,

<sup>a</sup>Department of Chemistry, Massachusetts Institute of Technology, Massachusetts 02139, USA. E-mail: jaj2109@mit.edu

<sup>b</sup>Koch Institute for Integrative Cancer Research, Massachusetts Institute of Technology, Cambridge, Massachusetts 02139, USA. E-mail: djirvine@mit.edu

† Electronic supplementary information (ESI) available: Detailed experimental procedures, spectral data, and supplementary figures. See DOI: 10.1039/d0sc02611e

‡ These authors contributed equally to this work.



where A and C are dissimilar, non-associating protein domains and B is a linker domain, eroded significantly more slowly than ABA or CBC hydrogels.<sup>33</sup> This result was rationalized based on the unique topology of the ABC network,<sup>34,35</sup> which cannot form mechanically defective primary loops.<sup>36,37</sup> Similarly, Lodge and coworkers reported linear ABC triblock copolymers with hydrophobic A, hydrophilic B, and thermoresponsive C blocks that formed micelles in water at room temperature and underwent physical gelation upon heating above the lower-critical solution temperature (LCST) of the C block (Fig. 1a). Here again, materials derived from ABC triblock copolymers were more mechanically robust than analogous ABA and CBC gels, presumably due to a reduction of primary loops.<sup>38,39</sup> Duvall and coworkers demonstrated the utility of linear ABC triblock copolymers with tunable degradation properties for controlled drug delivery applications.<sup>40,41</sup> Recently, Sheiko and coworkers reported on the development of linear–bottlebrush–linear “ABA” triblock copolymer elastomers where the central bottlebrush domain imbued the materials with strain stiffening behaviors analogous to biological tissues (Fig. 1b).<sup>42</sup> This study highlights the broad tunability of bottlebrush polymer networks, as variables such as grafting density, backbone length, and sidechain length all can be modified to achieve predictable material properties. Nevertheless, bottlebrush polymer materials based on the unique ABC topology (Fig. 1c) have not, to our knowledge, been reported in the context of supramolecular hydrogels, nor have they been examined in biomedical applications such as drug delivery. We envisioned that due to their unique ability to form multi-compartment networks, such materials could be especially useful as injectable hydrogels for local drug delivery. Unlike their ABA or AB counterparts, ABC copolymers enable separate micellization and gelation steps for straightforward drug encapsulation followed by formation of local drug depots at the site of injection,

respectively. In the context of cancer immunotherapy<sup>43–46</sup> where, for example, controlled release of agents that can generate cancer cell antigens and activate dendritic cells (DCs) selectively within the tumor microenvironment, ABC TBCs could significantly improve both the efficacy and safety of immunotherapies.<sup>47,48</sup>

With this goal in mind, we describe herein the design and synthesis of ABC TBCs *via* sequential ROMP of polylactic acid (PLA), polyethylene glycol (PEG), and poly(*N*-isopropylacrylamide) (PNIPAM) MMs (Fig. 2 and 3). Driven by the hydrophobicity of their PLA domains, TBCs with an ABC block sequence are shown to self-assemble in aqueous solutions at room temperature, forming uniform ~100 nm nanoparticles that can encapsulate and release small-molecule drugs (Fig. S1†) including paclitaxel (PTX), SN-38, resiquimod (R848), and gemcitabine, as well as a model protein (ovalbumin). Moreover, when heated above the LCST of PNIPAM (~32 °C), which is near physiological temperature (~37 °C), these TBC micelles rapidly formed hydrogels comprising a physically crosslinked network of hydrophobic PLA and PNIPAM domains connected by PEG domains (Fig. 1c and 2). TBC hydrogels loaded with PTX and R848 were administered intratumorally to immunocompetent mice bearing subcutaneous CT26 hind-flank tumors. The therapeutic index of the TBC hydrogel-based drug combination was improved compared to the combination of free PTX and R848, as determined by tumor volume measurements, quantification of systemic cytokines, and histology. In addition, cured mice re-challenged with CT26 cells did not develop new tumors, suggesting that the TBC hydrogel-mediated delivery facilitates an adaptive immune response. Altogether, this work establishes ABC TBCs as modular scaffolds for the formation of hydrogels with a range of potential controlled release applications.

## Design and synthesis of thermoresponsive TBC amphiphiles

To access the desired TBCs, we first prepared *exo*-norbornene imide-terminated MMs based on PLA (**Nb-PLA**), PEG (**Nb-PEG**), and PNIPAM (**Nb-PNIPAM**). **Nb-PLA** and **Nb-PEG** were synthesized following previously reported methods,<sup>49,50</sup> whereas **Nb-PNIPAM** was synthesized by coupling of commercially available 5.5 kDa amine-terminated PNIPAM to a previously reported norbornene-*N*-hydroxysuccinimidyl<sup>50</sup> ester (see ESI† for details). ROMP of these MMs was initiated by Grubbs 3<sup>rd</sup> generation bispyridyl complex (G3).

First, a TBC sample referred to as “ABC” was prepared through sequential copolymerization of **Nb-PLA**, **Nb-PEG**, and **Nb-PNIPAM** (Fig. 3a and Table 1). Size exclusion chromatography (SEC) traces obtained after consumption of **Nb-PLA** (red), **Nb-PEG** (blue) and **Nb-PNIPAM** (black) confirmed the incorporation of each block into ABC (Fig. 3b). Following quenching with excess ethyl vinyl ether (EVE), the reaction mixture was dialyzed against milliQ water (50 kDa molecular weight cutoff (MWCO) dialysis tubing), concentrated (using a 100 kDa MWCO centrifugal filter), and lyophilized to dryness. SEC analysis of the isolated ABC revealed a unimodal peak with no residual macromonomer (Fig. S2†). The number-average molar mass

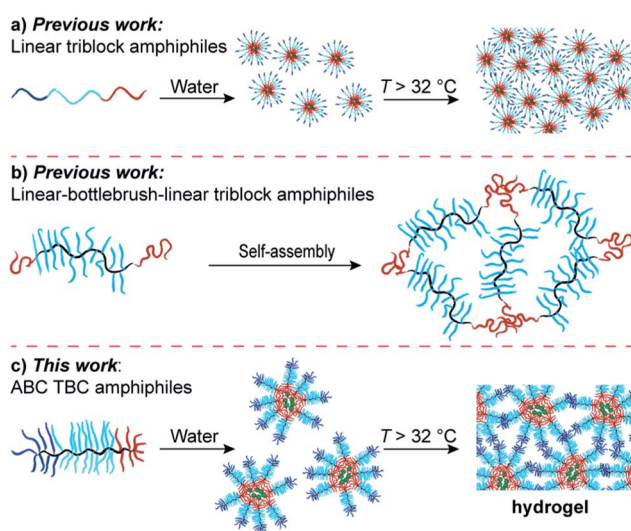


Fig. 1 (a) Linear triblock copolymer amphiphiles with thermoresponsive character. (b) Linear–bottlebrush–linear triblock copolymer networks (c) “ABC” triblock bottlebrush copolymer (TBC) amphiphiles and thermally responsive hydrogels described in this work.

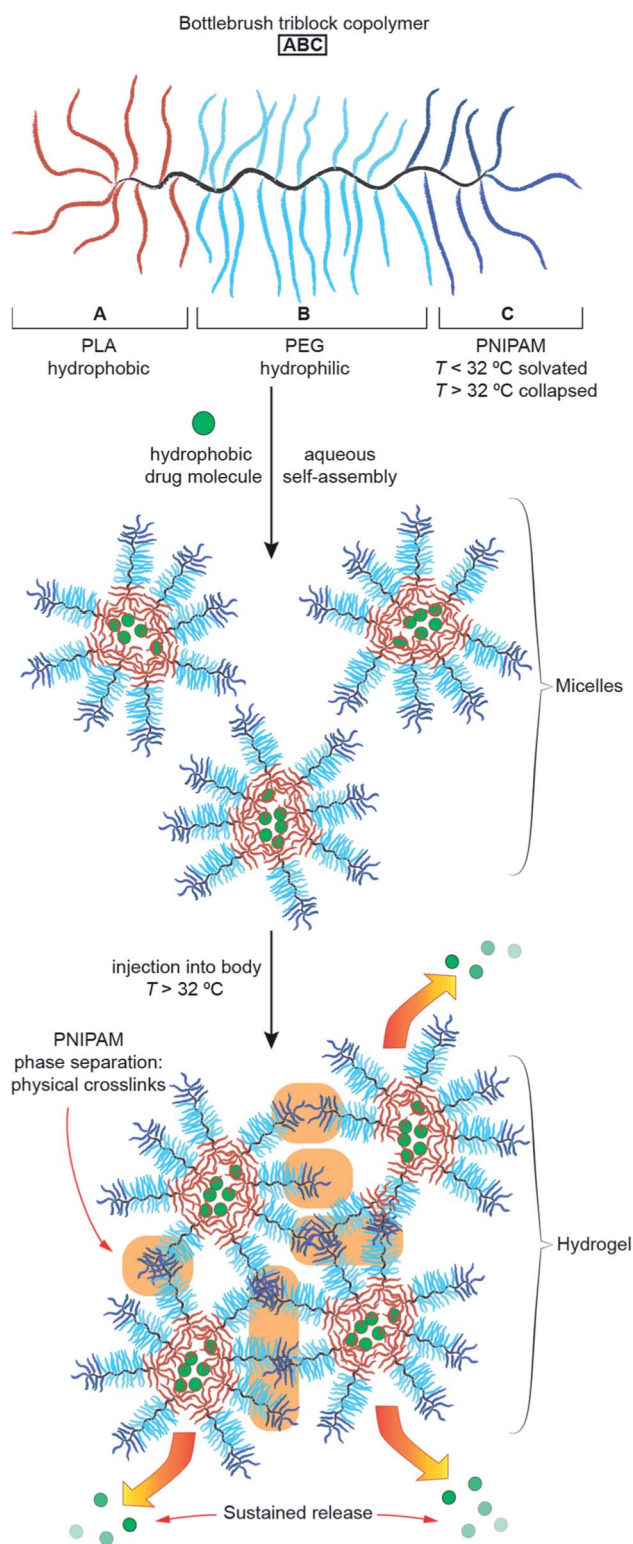


Fig. 2 Thermoresponsive ABC TBCs for local drug delivery. At room temperature, the TBCs self-assemble into micelles encapsulating hydrophobic drug molecules. Upon *in vivo* administration, PNIPAM phase separation induces hydrogel formation. Sustained, local release is achieved by diffusion of drug molecules from the hydrogel.

( $M_n$ ) of **ABC** was estimated by assuming complete conversion of **Nb-PLA** (as observed by SEC) and comparing the  $^1\text{H}$  NMR resonances for the PEG and PNIPAM segments to those of PLA (Fig. 3c and Table 1); close agreement between the MM feed ratios (e.g., theoretical  $M_n$ ) and experimentally measured block content was observed. To study the impact of block size and sequence on the properties of TBCs, a series of related copolymers was synthesized for comparison to **ABC**: “**CBA**” was prepared *via* sequential ROMP of the same MMs in the same ratios as **ABC** but in the reverse order; “**ABC-stat**” was synthesized by mixing the three MMs with **G3** providing a statistical copolymer with the same overall composition as **ABC**; lastly, a diblock bottlebrush copolymer “**AB**” lacking a PNIPAM block was synthesized as a non-thermoresponsive analogue of **ABC**. SEC,  $^1\text{H}$  NMR, differential scanning calorimetry (DSC), and thermogravimetric analysis (TGA) supported the proposed structures of these polymers (Table 1 and Fig. S3–S9<sup>†</sup>).

## Aqueous self-assembly and thermoresponsive behavior of TBCs

The solution self-assembly of these TBCs ( $1\text{ mg mL}^{-1}$  in water) was studied using dynamic light scattering (DLS) and transmission electron microscopy (TEM) (Fig. 4 and S10–S12<sup>†</sup>). Samples of TBC micelles were prepared by slow dilution of rapidly stirring DMSO solutions with water or saline buffer (to  $\sim 1\%$  DMSO by volume). Diblock **AB**, in contrast, was dissolved directly in water at  $50\text{ }^{\circ}\text{C}$  and no LCST behavior was observed. For these samples, DLS analysis revealed the presence of micelles with hydrodynamic diameters ( $D_h$ ) ranging from 90–119 nm (Table 2, Fig. 4a and S10<sup>†</sup>). As expected, **ABC** and **CBA** generated micelles of comparable sizes (113 nm, PDI: 0.05 and 120 nm, PDI: 0.07, respectively), consistent with their similar compositions. In addition, **AB** formed smaller micelles (93 nm, 0.08 PDI) as would be expected given its lack of a PNIPAM block. In contrast, **ABC-stat** formed considerably smaller ( $D_h = 45\text{ nm}$ , PDI: 0.17) assemblies compared to its TBC counterparts, highlighting the importance of sequence in programming TBC self-assembly. Variable-temperature DLS experiments revealed that dilute **ABC** micelles undergo reversible aggregation upon heating above the LCST of PNIPAM (Fig. S11<sup>†</sup>), presumably due to the formation of micelleplexes driven by PNIPAM hydrophobic interactions above its LCST.

Cryogenic transmission electron microscopy (cryoTEM) imaging confirmed the assembly of **ABC** into micelles with hydrophilic blocks forming a shell around well-resolved cores (Fig. 4b, c and S12<sup>†</sup>). The average micelle core size, as determined from the cryoTEM images, was  $20 \pm 3\text{ nm}$  (Fig. 4b). Assuming tight packing of the PLA blocks in the micelle cores and using the density of PLA ( $1.24\text{ g cm}^{-3}$ ), we estimate an average micelle is formed from approximately 100 TBC macromolecules.

Additionally, micelles derived from **ABC** were imaged by conventional TEM following drop-casting onto a carbon film-coated copper grid and negative staining (uranyl acetate), revealing particle sizes ( $102 \pm 19\text{ nm}$ ) that closely matched the

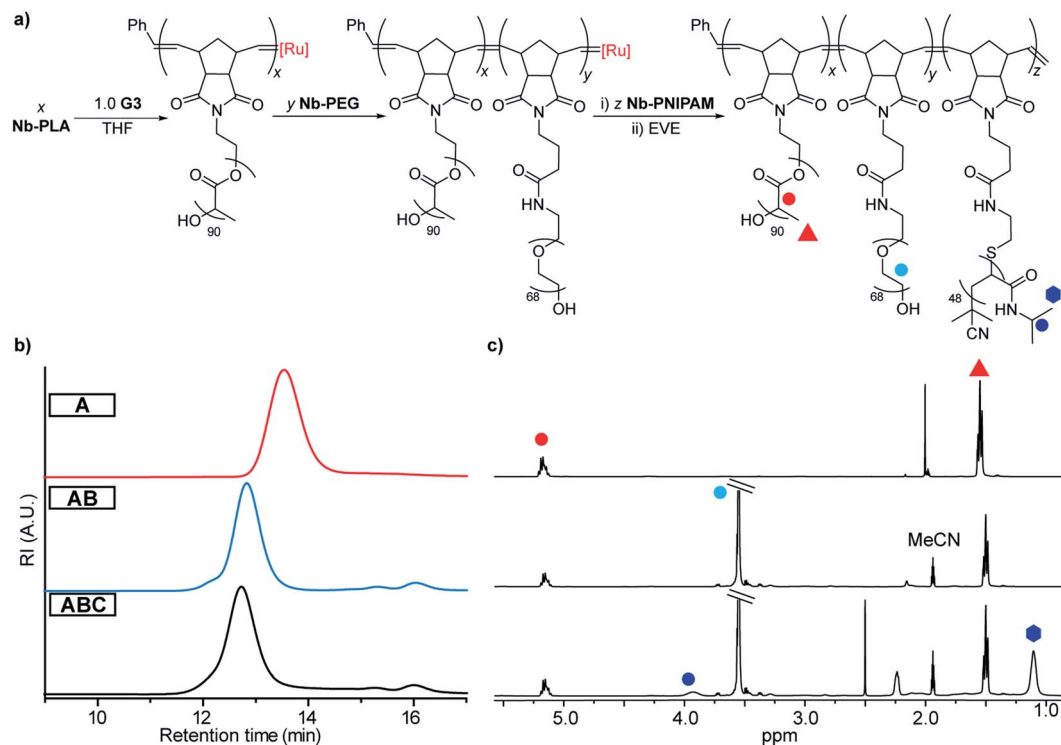


Fig. 3 (a) Sequential ROMP used for synthesis of TBCs. (b) Size-exclusion chromatography (SEC) analysis of sequential TBC growth. (c) Nuclear magnetic resonance ( $^1\text{H}$  NMR) of PLA bottlebrush polymer (A), PLA-*b*-PEG bottlebrush polymer (AB), and PLA-*b*-PEG-*b*-PNIPAM TBC (ABC).

$D_h$  values determined by DLS (Fig. 4d). When analogous samples were dried at an elevated temperature ( $>37$  °C) on the TEM grid, the formation of higher-order assemblies *via* fusion of micelles was directly observed (Fig. 4e).

Next, we investigated the thermally-induced gelation of aqueous solutions of a higher concentration (10 wt%) of ABC. At room temperature, the 10 wt% ABC solution is a clear liquid; upon heating to  $>32$  °C this solution converts into an opaque, free-standing hydrogel (Fig. 4f). Temperature sweep ( $1$  °C  $\text{min}^{-1}$ ) shear rheology demonstrated that at room temperature the 10 wt% ABC solution behaves like a viscous liquid with a greater loss modulus ( $G''$ ) than storage modulus ( $G'$ ) (Fig. 4g). Both  $G'$  and  $G''$  increased with increasing temperature, however, and  $G'$  increased much faster; the two values intersect at 36 °C, indicative of thermally induced gelation. At temperatures greater than 37 °C, the material behaves like a soft elastic solid ( $G' > G''$ ).

Characterization of ABC solutions using small angle X-ray scattering (SAXS) painted a similar picture. At room temperature, the scattering profile of an aqueous solution of ABC

(10 wt%) displayed a group of broad peaks at low  $q$  values ( $q < 0.02$   $\text{\AA}^{-1}$ , red box in Fig. 4h) that are assigned to the structural factors, which are related to the inter-particle spatial relationship. The inter-domain spacing ( $d$ ) calculated using  $d = 2\pi/q$  was found to be  $\sim 60$  nm, which suggests that the hydrophilic shells of these ABC micelles ( $D_h = 110$  nm) overlap at this concentration (10 wt%). As expected,  $d$  correlated inversely with ABC micelle concentration (Fig. S13 $^\dagger$ ). The small peaks in the higher  $q$  region (green box in Fig. 4d) are attributed to the form factor of the PLA core. By fitting with a hard sphere model, the average core radius was estimated to be  $\sim 9$  nm, which agrees well with the cryoTEM results (Fig. 4b). Temperature-dependent SAXS revealed clear changes in the scattering curves, most notably a shift of the structure factor peaks to higher  $q$  (smaller  $d$ ), which is likely a consequence of the collapse of the PNIPAM phase and inter-micelle crosslinking. Upon cooling the sample, the SAXS profile returned to nearly the same form as in the initial state, indicating that the shape and size of the micelles

Table 1 Compositions of bottlebrush copolymers

Entry	Copolymer	$N_{(\text{PLA } 6.6 \text{ k})}^a$	$N_{(\text{PEO } 3 \text{ kDa})}^b$	$N_{(\text{PNIPAM } 5.5 \text{ k})}^b$	$M_n$ ( $\text{kg mol}^{-1}$ ) <sup>b</sup>	$D$
AB	PLA- <i>b</i> -PEG	7.6	43.2	—	179	1.12
ABC	PLA- <i>b</i> -PEG- <i>b</i> -PNIPAM	7.6	43.8	8.6	229	1.25
CBA	PNIPAM- <i>b</i> -PEG- <i>b</i> -PLA	7.6 <sup>a</sup>	40 <sup>a</sup>	10 <sup>a</sup>	225	1.35
ABC- <i>stat</i>	PLA- <i>co</i> -PEG- <i>co</i> -PNIPAM	7.6	41.4	8.2	219	1.21

<sup>a</sup> Assumed quantitative incorporation based on SEC analysis. <sup>b</sup> Based on  $^1\text{H}$  NMR peak integrations relative to PLA content.

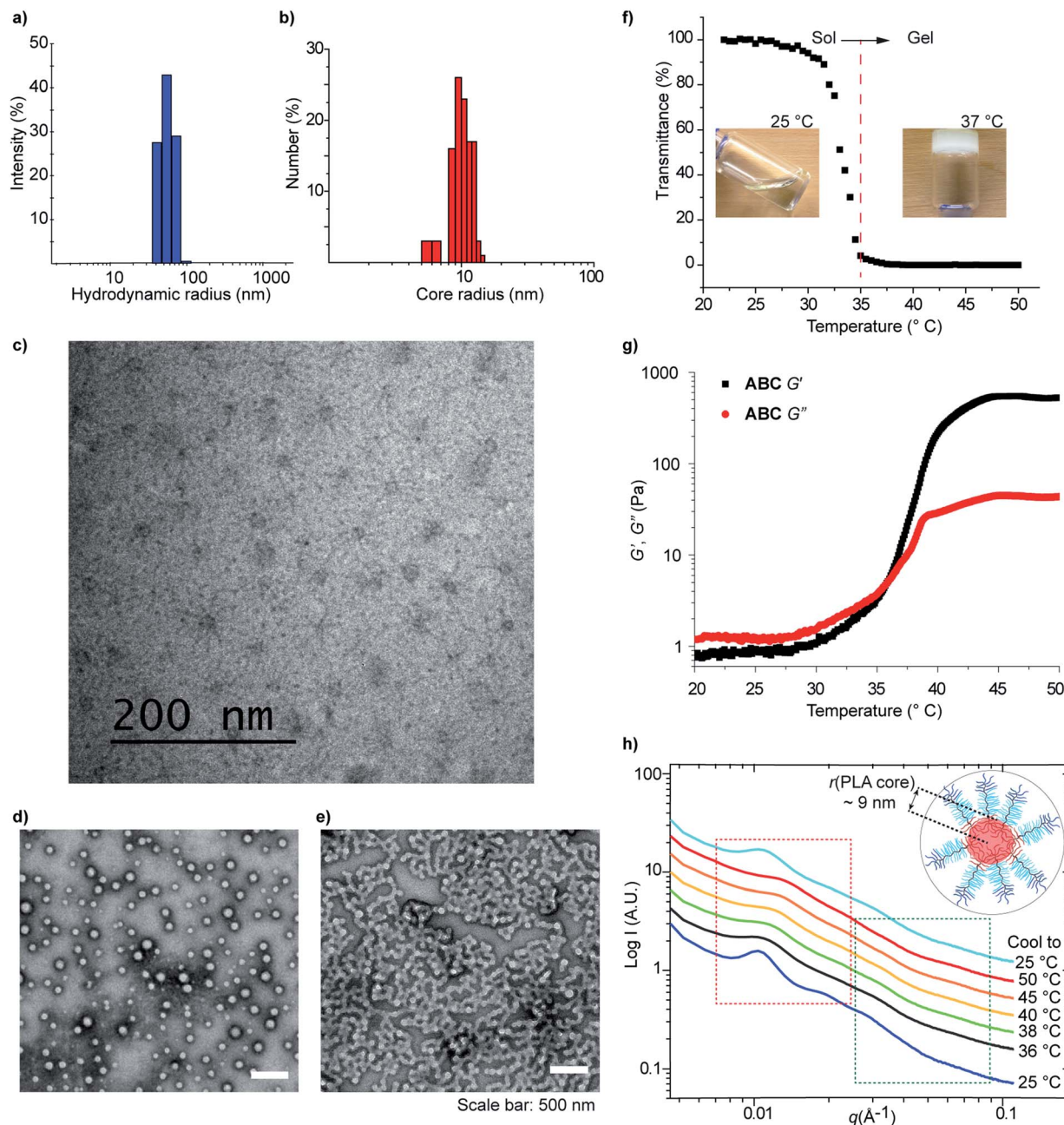


**Fig. 4** (a) DLS analysis of aqueous self-assembly of **ABC** triblock copolymer. (b) Core size distribution of micelles of **ABC** TBC measured from cryoTEM images. (c) **ABC** micellar solution imaged in native state by cryoTEM. (d and e) TEM images of dilute **ABC** micelle solutions prepared with  $\text{UO}_2(\text{OAc})_2$  stain at 25 °C and 37 °C. (f) Temperature-dependent light transmission (640 nm) of **ABC** micellar solution (10 wt%). (g) Temperature sweep rheology of **ABC** micellar solution (10 wt%). (h) Variable-temperature small-angle X-ray scattering (SAXS) curves of **ABC** micellar solution (10 wt%).

are maintained following heating and cooling and that the gelation process is reversible.

Lastly, thermal gelation of **ABC** was investigated *in vivo*. A solution (10 wt% in saline buffer) of fluorescently labeled (cyanine 7.5) TBC sample “**ABC-Cy7.5**” was injected subcutaneously into the hind flank of healthy balb/c mice ( $n = 3$ ) with their hair shaved around the injection site. The mice were imaged (IVIS;  $\lambda_{\text{ex/em}} = 745/800$  nm) shortly after injection and again after 24 h. A fluorescently labeled diblock bottlebrush

“**AB-Cy7.5**” lacking a PNIPAM domain was used as a control sample. Fig. S14† shows that **ABC-Cy7.5** formed a localized patch at the injection site with no signs of spreading after 24 h. In contrast, after 24 h **AB-Cy7.5** had diffused from the injection site throughout the imageable, shaved region. Taken together, these results suggest that at physiological temperature ( $\sim 37$  °C), **ABC-Cy7.5** forms a physical hydrogel that remains at the injection site while its diblock counterpart does not, suggesting that

Table 2 Aqueous self-assembly and drug encapsulation efficiency of bottlebrush copolymers

Micelle	$D_h$ (nm)	PDI	Encapsulation efficiency <sup>a</sup> (%)
<b>AB</b>	93	0.08	—
<b>ABC</b>	113	0.05	—
<b>CBA</b>	120	0.07	—
<b>ABC-stat</b>	45	0.17	—
Dexamethasone/ <b>ABC</b>	92	0.1	78
Ibuprofen/ <b>ABC</b>	108	0.09	65
Ofloxacin/ <b>ABC</b>	113	0.16	63
Paclitaxel (PTX)/ <b>ABC</b>	104	0.14	91
Resiquimod (R848)/ <b>ABC</b>	118	0.15	71

<sup>a</sup> Drug encapsulation efficiency based on % of drug (5 mg) retained in **ABC** TBC (50 mg).

the former material could be particularly useful for local drug delivery applications.

## Biocompatibility and drug loading

We have previously reported on soluble PEG-based bottlebrush polymers prepared *via* ROMP;<sup>51,52</sup> these materials have displayed excellent safety profiles, including in liver and kidney function panels, following systemic administration in mice, rats and dogs. Here, in preparation for *in vivo* local drug delivery studies, we investigated the *in vitro* toxicity and drug release properties of our **ABC** hydrogels. Polymeric amphiphiles are often employed to permeabilize cell membranes;<sup>53</sup> thus, it was important to determine if **ABC** causes cell membrane damage that could trigger an undesired inflammatory response. Aqueous solutions of **ABC** were incubated with human umbilical vein endothelial cells (HUVEC) for 48 h and the cell culture media was assayed for free lactate dehydrogenase (LDH), which is typically only found in the cytosol of healthy cells and thus represents a biomarker for cell membrane integrity. Polyethylenimine (PEI), a cationic polymer that destabilizes cell membranes, and cell lysate were used as positive controls. Gratifyingly, cells incubated with **ABC** released negligible amounts of LDH, comparable to the levels detected for untreated cells (Fig. S15<sup>†</sup>), suggesting that **ABC** does not induce rupture of HUVEC cells.

Next, we examined the encapsulation and release of seven small-molecule drugs (dexamethasone, ibuprofen, ofloxacin, SN-38, paclitaxel, gemcitabine, and R848) and a model ~45 kDa protein (fluorescently labeled ovalbumin, OVA) from **ABC** hydrogels. A straightforward drug encapsulation protocol was developed, where known amounts of dry **ABC** and a given drug were dissolved in dimethyl sulfoxide (DMSO) and then slowly diluted with saline buffer to obtain an aqueous solution with ≤1% organic solvent. The drug-loaded micellar solutions were then spin-concentrated to a TBC concentration of ~10 wt% where they behaved as free-flowing fluids at room temperature. The drug encapsulation efficiency was determined using liquid chromatography-mass spectrometry (LC-MS) (Table 2 and Fig. S1<sup>†</sup>). Importantly, the drug-loaded **ABC** solutions retained their ability to undergo rapid gelation upon warming to 37 °C.

The extent of drug release *versus* time at 37 °C was assessed by placing the drug-loaded **ABC** hydrogel inside a dialysis membrane (50 kDa MWCO) and measuring the amount of free drug in the exterior saline solution *via* LC-MS for small molecules or UV-vis for OVA (Fig. S16<sup>†</sup>).

While the encapsulation efficiencies of the individual drugs somewhat correlated with their lipophilicity values ( $\log D$ , Fig. S1<sup>†</sup>), *i.e.*, the more hydrophobic drugs were encapsulated more efficiently, release was comparable for all drugs—linear release profiles with apparent half-lives of ~3–5 days were observed. Gratifyingly, **ABC** hydrogel also provided sustained release of the model protein payload, OVA-FITC, suggesting potential applications of this platform for improving the therapeutic index of cytokines and checkpoint inhibitors *via* prolonged intratumor retention. While we note that these release rates could perhaps be extended by altering the composition of **ABC**, our results suggest that the presently studied **ABC** hydrogels are capable of encapsulating and providing controlled release of a range of drugs with varying molecular structures and pharmacological properties.

## Immunochemotherapy studies

Having established that **ABC** hydrogels achieve sustained release of drugs at physiological temperatures *in vitro*, we decided to evaluate the ability of this material to facilitate local release of therapies that activate the immune system. The immune system has been implicated in the efficacy of chemotherapeutics,<sup>54–56</sup> lending to potential synergy when chemotherapy is combined with additional immune activation. For example, PTX, a canonical microtubule inhibitor, has been shown to enhance DC maturation, cross-presentation of antigen, depletion of myeloid-derived suppressor cells, and tumor penetration by cytotoxic T cells and natural killer (NK) cells—all factors contributing to its anti-tumor effects.<sup>57–60</sup> Given the immunomodulatory effects of chemotherapy and the release of tumor cell antigens following chemotherapy-induced cell death, it has long been reasoned that combinations of chemotherapy and immunomodulators like TLR agonists may display improved tumor efficacy.<sup>61–63</sup> Unfortunately, when administered systemically, TLR agonists can induce dramatic flu-like symptoms and related short and long-term side-effects collectively described as cytokine release syndrome.<sup>64,65</sup> To minimize systemic side effects, drugs with immune-activating mechanisms of action are often administered locally directly into the accessible tumors.<sup>66,67</sup> Intratumoral administration, however, does not completely prevent the systemic dissemination of small molecule TLR agonists that can rapidly drain into the vasculature due to their small molecular sizes and the high interstitial pressure within tumors.<sup>68</sup> Additionally, repetitive administration of high doses of immunomodulators can lead to TLR-tolerance,<sup>69–71</sup> a phenomenon that might explain tachyphylaxis and the limited effectiveness of free TLR7/8 ligands in early human trials.<sup>64,65,72</sup> Thus, sustained local delivery is a promising approach to balance the efficacy and side-effects of TLR agonists. To prevent adverse events caused by systemic exposure and to overcome limited efficacy in clinical

immunotherapy, research labs both in academia and pharmaceutical companies are exploring ways to achieve prolonged retention of immunomodulators, such as the use of PEG-<sup>73</sup> or lipid conjugation,<sup>46,72</sup> and aluminum oxide adsorption.<sup>74</sup>

We reasoned that the **ABC** hydrogel could deliver a combination of R848 and PTX in a sustained fashion, producing a localized anti-tumor immune response while at the same time reducing whole body exposure to these potent molecules. R848 and PTX were chosen based on work from Linnebacher and coworkers showing the superior activity of this combination against colon cancer compared to the first-line medication irinotecan.<sup>75</sup> Taking advantage of the straightforward drug formulation protocol described above, we loaded **ABC** micelles with a mixture of R848 and PTX and evaluated the efficacy of the resulting material in balb/c mice ( $n = 10$  per group) bearing subcutaneous CT26 colon cancer tumors on their hind flank. The CT26 model is a syngeneic tumor model widely used for testing of immunotherapies in immunocompetent mice. We note that all animal studies were conducted under federal, state, and local guidelines in accordance with the Public Health Service Policy on Humane Care and Use of Laboratory Animals and the National Institutes of Health Guide for the Care and Use of Laboratory Animals with approval from the Massachusetts Institute of Technology Committee on Animal Care.

Two different **ABC** micelles with encapsulated PTX and different amounts of R848: **ABC-1** (1.5 mg kg<sup>-1</sup> of R848 + 10 mg kg<sup>-1</sup> of PTX) and **ABC-2** (3 mg kg<sup>-1</sup> of R848 + 10 mg kg<sup>-1</sup> of PTX), were injected intratumorally every five days for 10 d (3 total injections); tumor volumes and mouse survival were plotted as a function of time for up to 75 d, while the “study readout,” taken as the last day of survival of mice treated with saline as a control, was 48 d. Additional control groups included mice given non-drug-loaded **AB** (“**AB** blank”), non-drug-loaded **ABC** (“**ABC** blank”), the 1× dose PTX and R848 used above but in 75% DMSO/PBS (“free R848 + PTX”), and 1× dose of PTX and R848 used above but in the non-gelling diblock copolymer **AB** (“**AB-1**”).

While the PTX + R848 combination conferred a clear survival advantage over saline, **AB** blank, and **ABC** blank, differences between the four treatment groups (free drugs, **AB-1**, **ABC-1**, and **ABC-2**) were not apparent from the average survival curve alone (Fig. 5a), which cannot distinguish between animals that display delayed tumor growth *versus* cures. To highlight differences between these groups at the study readout time (48 d), plots of tumor area for each mouse (Fig. 5b–h) were color-coded by non-responders (red lines), limited responders (black lines), and cures (green lines). From these plots, it is clear that the tumors in mice from the saline (Fig. 5b), **AB** blank (Fig. 5c), and **ABC** blank (Fig. 5d) groups all grew at roughly equal rates with the exception one limited responder from the **ABC** blank cohort. Additionally, while both the free drug (Fig. 5e) and **AB-1** (Fig. 5f) groups displayed improved efficacy, they were dominated by non-responders (3 and 2, respectively) and limited responders (6 and 7, respectively) with only 1 cure per group. In sharp contrast, the **ABC-1** (Fig. 5g) and **ABC-2** (Fig. 5h) groups had 8 and 7 cures (Fig. 5i), respectively, suggesting that the hydrogel-

mediated local delivery strategy confers an efficacy advantage through an increase in the number of mice cured per group.

Less frequent, fractionated dosing of TLR7/8 agonist over several hours was found to avert the onset of systemic TLR-tolerance, improving anticancer efficacy of the immunomodulator relative to its bolus injections.<sup>70</sup> Therefore, it is reasonable that slow-releasing **ABC** formulations elicit faster antitumor activity by providing controlled generation of tumor antigens by PTX synchronized with sustained local activation of innate immune cells by R848.<sup>76</sup> Properly timed activation of innate immune cells, including dendritic cells, leads to the processing and presentation of tumor-derived antigens to T cells, generating a potent tumor-specific immune response capable of fast eradication of tumors and the potential for long-lasting memory against tumor recurrence. Indeed, it was found that mice cured from the initial **ABC-1** therapy had acquired immune memory against CT26 tumors: long-term surviving mice from the previous efficacy study ( $n = 5$ ) were re-challenged with CT26 tumor cells on their opposite hind flank. Over the course of several weeks after cell implantation, no tumor growth was observed; all tumors were rejected (Fig. S18a†). As a control, naïve mice were inoculated with the same number of cells; rapid tumor outgrowth occurred. In a separate study, groups of mice ( $n = 5$  animals per group) were treated intratumorally with only R848 formulated in **ABC** or as free drug solution. Three weeks after a single injection the presence of circulating tumor antigen-specific CD8<sup>+</sup> T cells was confirmed (Fig. S17b†), further corroborating the induction of tumor-specific immune responses *via* intratumoral injection of R848. Remarkably, the levels of antigen-specific CD8<sup>+</sup> T cells trended slightly higher in mice treated with R848 formulated in **ABC** compared to free or **AB** formulated R848, though all treated mice had elevated tumor-specific T cell levels in circulation.

In addition to the improved efficacy observed above for **ABC** hydrogel mediated R848 delivery, we noted visible inflammation at the site of injection of the free drug combination that was not present for the **ABC** hydrogel groups (Fig. 6a and S18†). This observation suggested that without **ABC** hydrogel, the free drug combination induces local inflammation that takes considerably longer to clear. Histological analyses of tissue samples from the group administered the free drug combination were conducted to assay for signs of chronic inflammation associated with topically applied immune stimulators.<sup>77,78</sup> As shown in Fig. 6a these mice showed signs of chronic inflammation that still persisted at 60 d, while the tumors were completely cured in the **ABC** treatment groups (Fig. S18†). Despite the intact epidermis and dermis, histological analysis revealed collagen buildup within the hypodermis of the free-drug-treated mice, indicative of scar tissue formation (Fig. 6b–d and S19a†). Moreover, extensive macrophage infiltration was noted beneath the skin (Fig. 6c), while lymphocyte and granulocyte accumulation was also present at the site of the scar (Fig. 6d). Meanwhile, no visible signs of chronic inflammation were detected in the **ABC** hydrogel groups (Fig. S18†).

To assay for undesired systemic inflammation, serum samples collected 6 h after the first intratumoral injection were assayed for four cytokines—MCP-1, IL-12, IL-6, and TNF—that are produced by dendritic cells and macrophages upon TLR-7/8

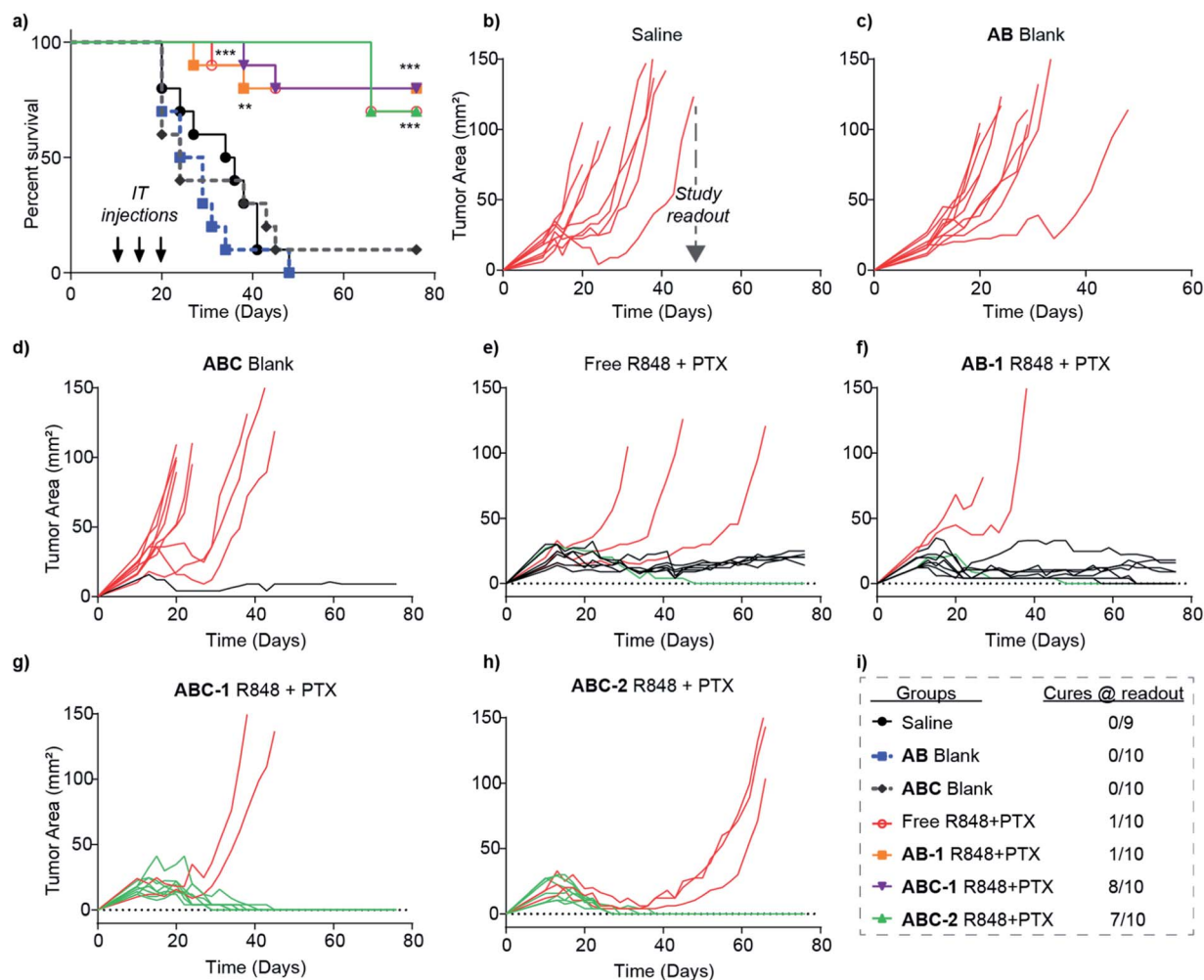


**Fig. 5** Survival (a) and CT26 tumor growth (b–h) in treatment groups of balb/c mice ( $n = 10$ ). Mice were intratumorally administered R848 at 1.5 (1) or 3 mg mL<sup>-1</sup> (2) in combination with 10 mg kg<sup>-1</sup> PTX formulated in ABC, AB, or DMSO/saline. Control groups received equal volumes of PBS or blank bottlebrush polymer solutions. Mice in groups are color-coded by non-responders (red lines), limited responders (black lines), and cures (green lines). (i) Efficacy endpoint based on the time of complete loss of the saline control group to the tumor burden. Statistical significance was determined using log-rank (Mantel Cox) test, differences amongst treatment groups compared to saline group have been denoted with \*\* for  $p < 0.005$  and with \*\*\* for  $p < 0.0005$ .

activation and thus serve as biomarkers for systemic immune activation (Fig. 6e–h). In support of our hypothesis, 2–3-fold lower levels of MCP-1, IL-12, and IL-6 were measured for the ABC-1 group compared to the free drug group. Moreover, the ABC-2 group, which received twice the amount of R848 overall, displayed similar cytokine levels as the 1× free drug group, showing that the local delivery strategy can facilitate the use of higher doses with comparable systemic side effects. Interestingly, even the AB-encapsulated PTX-R848 combination led to lower amounts of systemic cytokines compared to the free drug group, likely due to the lower bioavailability of the encapsulated drug. As expected, no increased cytokine production was detected in the control groups. Altogether, these data show the advantage of our TBC hydrogel for local R848 and PTX delivery, leading to both an increase in efficacy (Fig. 5) and improved safety (Fig. 6), which translate to an overall improved therapeutic index.

The reduction of systemic cytokines using ABC hydrogels is likely due to prevention of burst exposure of R848 (Fig S14 and

S16†). These results align with a pharmaceutical industry-wide shift toward immunomodulator formulations that retain the drug at the site of injection, thus enhancing therapeutic index.<sup>72–74</sup> In addition to induction of higher unwanted systemic inflammatory cytokines, intratumoral injections of free R848 + PTX resulted in delayed cures with persistent inflammation at the injection site, which are likely caused by burst exposure to PTX with subsequent massive antigen release occurring after a majority of the R848 immunomodulator has diffused away from the site of injection, promoting tolerance.<sup>56,79</sup> Indeed, it has been previously demonstrated that improper timing of immune activation and antigen release can significantly dampen antitumor immune responses.<sup>80</sup> We also observed higher systemic levels of the anti-inflammatory cytokine IL-10 for longer periods in mice given the free drug combination (Fig. S19b†), which could partially explain delayed clearing of the tumors.<sup>81</sup>



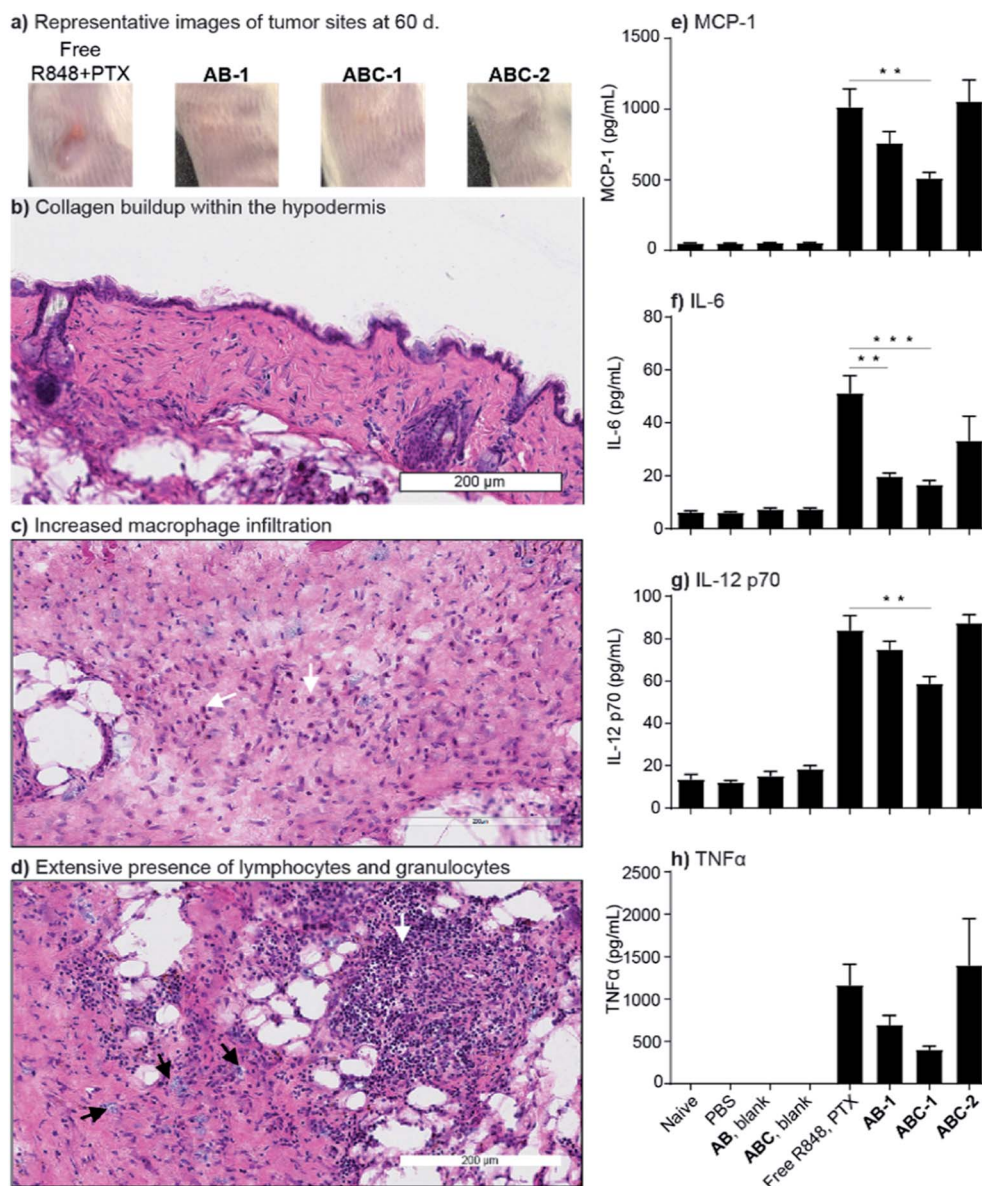


**Fig. 6** (a) Representative images of tumor sites in treatment groups at 60 days. Histology of injection site in a mouse in the free drugs treatment group showing signs of chronic inflammation (b) collagen under intact dermis, (c) heightened macrophage infiltration, (d) and extensive presences of lymphocytes and granulocytes. Serum cytokine levels in mice groups ( $n = 10$ ) 6 hours after intratumoral injection of formulations of R848 and PTX: (e) monocyte chemoattractant protein-1, MCP-1; (f) Interleukin 6, IL-6; (g) Interleukin 12, IL-12p70; (h) tumor necrosis factor, TNF $\alpha$ . Statistical significance was determined using one-way ANOVA followed by *post hoc* Dunnett's multiple comparisons test, differences amongst treatment groups compared to free R848, PTX group; \*\* for  $p < 0.005$  and with \*\*\* for  $p < 0.0005$ .

The narrow therapeutic indices of systemically administered traditional chemotherapeutics give rise to their well-known side effects. Similar challenges are surfacing in the promising field of immunochemotherapy, motivating the development of intratumoral delivery strategies. Wide adoption of such combination therapies, however, demands the availability of smart vehicles for local drug delivery that are capable of maintaining optimal concentrations of chemotherapeutics and immunomodulators in tumor tissue to achieve curing effects without producing tolerogenic or unwanted side effects. Our results demonstrate that TBC-based hydrogels enable delivery of a combination of a chemotherapeutic (PTX) and a TLR7/8

agonist (R848), promoting tumor-controlling immunologic effects while reducing dose-limiting systemic and local toxicities associated with such therapies.

## Conclusions

We developed an effective protocol for the synthesis of modular TBCs. Using a range of physicochemical characterization techniques, we demonstrate that "ABC" sequenced TBCs self-assemble into well-defined stable micelles at room temperature, allowing for efficient encapsulation of variety of bioactive payloads. We further show that at physiological temperatures ( $T$

> 32 °C), aqueous solutions of ABC TBCs undergo rapid gelation, forming a localized depot for sustained release of encapsulated therapeutics. These TBC amphiphiles represent a universal platform for local drug delivery, with efficient drug encapsulation, straightforward formulation and administration, and the ability to provide sustained release for both small molecule drugs and macromolecular payloads, properties that bode well for future applications in areas ranging from anti-cancer chemo- and immunotherapy to ophthalmic therapy.

## Abbreviations

PLA	Poly(lactic acid)
PEG	Poly(ethylene glycol)
PNIPAM	Poly( <i>N</i> -isopropylacrylamide)
LCST	Lower critical solution temperature
$T_g$	Glass transition temperature
ROMP	Ring-opening metathesis polymerization

## Author contributions

The manuscript was written through contributions of all authors. All authors have given approval to the final version of the manuscript.

## Funding sources

JAJ acknowledges support from the National Institutes of Health (1R01CA220468-01) and London Eye Hospital Pharma. LEM is supported by the National Institutes of Health NIGMS Interdepartmental Biotechnology Training Program (T32-GM008334). This work was supported in part by the Marble Center for Nanomedicine and the Koch Institute Support (core) Grant P30-CA14051. DJI is an investigator of the Howard Hughes Medical Institute.

## Conflicts of interest

There are no conflicts of interest to declare.

## Acknowledgements

X-ray scattering experiments were performed at the Advanced Photon Source, a U.S. Department of Energy (DOE) Office of Science User Facility operated for the DOE Office of Science by Argonne National Laboratory (DE-AC0206CH11357).

## References

- W. F. M. Daniel, J. Burdyńska, M. Vatankhah-Varnoosfaderani, K. Matyjaszewski, J. Paturej, M. Rubinstein, A. V. Dobrynin and S. S. Sheiko, Solvent-free, supersoft and superelastic bottlebrush melts and networks, *Nat. Mater.*, 2016, **15**, 183.
- M. Alaboalirat, L. Qi, K. J. Arrington, S. Qian, J. K. Keum, H. Mei, K. C. Littrell, B. G. Sumpter, J.-M. Y. Carrillo, R. Verduzco and J. B. Matson, Amphiphilic Bottlebrush Block Copolymers: Analysis of Aqueous Self-Assembly by Small-Angle Neutron Scattering and Surface Tension Measurements, *Macromolecules*, 2019, **52**, 465.
- G. M. Miyake, V. A. Piunova, R. A. Weitekamp and R. H. Grubbs, Precisely Tunable Photonic Crystals From Rapidly Self-Assembling Brush Block Copolymer Blends, *Angew. Chem., Int. Ed.*, 2012, **51**, 11246.
- M. A. Sowers, J. R. McCombs, Y. Wang, J. T. Paletta, S. W. Morton, E. C. Dreaden, M. D. Boska, M. F. Ottaviani, P. T. Hammond, A. Rajca and J. A. Johnson, Redox-responsive branched-bottlebrush polymers for in vivo MRI and fluorescence imaging, *Nat. Commun.*, 2014, **5**, 5460.
- J. A. Johnson, Y. Y. Lu, A. O. Burts, Y. Xia, A. C. Durrell, D. A. Tirrell and R. H. Grubbs, Drug-Loaded, Bivalent-Bottle-Brush Polymers by Graft-through ROMP, *Macromolecules*, 2010, **43**, 10326.
- H. Unsal, S. Onbulak, F. Calik, M. Er-Rafik, M. Schmutz, A. Sanyal and J. Rzayev, Interplay between Molecular Packing, Drug Loading, and Core Cross-Linking in Bottlebrush Copolymer Micelles, *Macromolecules*, 2017, **50**, 1342.
- S. S. Sheiko, B. S. Sumerlin and K. Matyjaszewski, Cylindrical molecular brushes: Synthesis, characterization, and properties, *Prog. Polym. Sci.*, 2008, **33**, 759.
- J. Bolton and J. Rzayev, Tandem RAFT-ATRP Synthesis of Polystyrene-Poly(Methyl Methacrylate) Bottlebrush Block Copolymers and Their Self-Assembly into Cylindrical Nanostructures, *ACS Macro Lett.*, 2012, **1**, 15.
- J. C. Foster, S. Varlas, B. Couturaud, Z. Coe and R. K. O'Reilly, Getting into Shape: Reflections on a New Generation of Cylindrical Nanostructures' Self-Assembly Using Polymer Building Blocks, *J. Am. Chem. Soc.*, 2019, **141**, 2742.
- R. Verduzco, X. Li, S. L. Pesek and G. E. Stein, Structure, function, self-assembly, and applications of bottlebrush copolymers, *Chem. Soc. Rev.*, 2015, **44**, 2405.
- Y. Xia, B. D. Olsen, J. A. Kornfield and R. H. Grubbs, Efficient Synthesis of Narrowly Dispersed Brush Copolymers and Study of Their Assemblies: The Importance of Side Chain Arrangement, *J. Am. Chem. Soc.*, 2009, **131**, 18525.
- L. Su, G. S. Heo, Y.-N. Lin, M. Dong, S. Zhang, Y. Chen, G. Sun and K. L. Wooley, Syntheses of triblock bottlebrush polymers through sequential ROMPs: Expanding the functionalities of molecular brushes, *J. Polym. Sci., Part A: Polym. Chem.*, 2017, **55**, 2966.
- Z. Li, K. Zhang, J. Ma, C. Cheng and K. L. Wooley, Facile syntheses of cylindrical molecular brushes by a sequential RAFT and ROMP "grafting-through" methodology, *J. Polym. Sci., Part A: Polym. Chem.*, 2009, **47**, 5557.
- Y. Li, J. Zou, B. P. Das, M. Tsianou and C. Cheng, Well-Defined Amphiphilic Double-Brush Copolymers and Their Performance as Emulsion Surfactants, *Macromolecules*, 2012, **45**, 4623.
- K. Kawamoto, M. Zhong, K. R. Gadelrab, L.-C. Cheng, C. A. Ross, A. Alexander-Katz and J. A. Johnson, Graft-

- through Synthesis and Assembly of Janus Bottlebrush Polymers from A-Branch-B Diblock Macromonomers, *J. Am. Chem. Soc.*, 2016, **138**, 11501.
- 16 H. V. T. Nguyen, A. Detappe, N. M. Gallagher, H. Zhang, P. Harvey, C. Yan, C. Mathieu, M. R. Golder, Y. Jiang, M. F. Ottaviani, A. Jasanoff, A. Rajca, I. Ghobrial, P. P. Ghoroghchian and J. A. Johnson, Triply Loaded Nitroxide Brush-Arm Star Polymers Enable Metal-Free Millimetric Tumor Detection by Magnetic Resonance Imaging, *ACS Nano*, 2018, **12**, 11343.
- 17 Z. Li, J. Ma, C. Cheng, K. Zhang and K. L. Wooley, Synthesis of Hetero-Grafted Amphiphilic Diblock Molecular Brushes and Their Self-Assembly in Aqueous Medium, *Macromolecules*, 2010, **43**, 1182.
- 18 G. Dumortier, J. L. Grossiord, F. Agnely and J. C. Chaumeil, A Review of Poloxamer 407 Pharmaceutical and Pharmacological Characteristics, *Pharm. Res.*, 2006, **23**, 2709.
- 19 P. Lundberg, N. A. Lynd, Y. Zhang, X. Zeng, D. V. Krogstad, T. Paffen, M. Malkoch, A. M. Nyström and C. J. Hawker, pH-triggered self-assembly of biocompatible histamine-functionalized triblock copolymers, *Soft Matter*, 2013, **9**, 82.
- 20 H. Otsuka, Y. Nagasaki and K. Kataoka, Self-assembly of poly(ethylene glycol)-based block copolymers for biomedical applications, *Curr. Opin. Colloid Interface Sci.*, 2001, **6**, 3.
- 21 E. M. Saffer, G. N. Tew and S. R. Bhatia, Poly(lactic acid)-poly(ethylene oxide) Block Copolymers: New Directions in Self-Assembly and Biomedical Applications, *Curr. Med. Chem.*, 2011, **18**, 5676.
- 22 C. M. Bates, A. B. Chang, N. Momčilović, S. C. Jones and R. H. Grubbs, ABA Triblock Brush Polymers: Synthesis, Self-Assembly, Conductivity, and Rheological Properties, *Macromolecules*, 2015, **48**, 4967.
- 23 Y. Yamauchi, K. Yamada and Y. Ishida, Synthesis of Water-soluble Bottlebrush Polymer with Hydrophobic Core and Hydrophilic Shell as Cylindrical Host for Guest Uptake, *Chem. Lett.*, 2019, **48**, 1410.
- 24 T. Pelras, C. S. Mahon and M. Müllner, Synthesis and Applications of Compartmentalised Molecular Polymer Brushes, *Angew. Chem., Int. Ed.*, 2018, **57**, 6982.
- 25 F. Shao, Y. Wang, C. M. Tonge, E. R. Sauvé and Z. M. Hudson, Self-assembly of luminescent triblock bottlebrush copolymers in solution, *Polym. Chem.*, 2020, **11**, 1062.
- 26 Y. Yamauchi, K. Yamada, N. N. Horimoto and Y. Ishida, Supramolecular self-assembly of an ABA-Triblock bottlebrush polymer: Atomic-force microscopy visualization of discrete oligomers, *Polymer*, 2017, **120**, 68.
- 27 I. Lyubimov, M. G. Wessels and A. Jayaraman, Molecular Dynamics Simulation and PRISM Theory Study of Assembly in Solutions of Amphiphilic Bottlebrush Block Copolymers, *Macromolecules*, 2018, **51**, 7586.
- 28 Y. Chen, H. Zhou, Z. Sun, H. Li, H. Huang, L. Liu and Y. Chen, Shell of amphiphilic molecular bottlebrush matters as unimolecular micelle, *Polymer*, 2018, **149**, 316.
- 29 A. B. Chang, C. M. Bates, B. Lee, C. M. Garland, S. C. Jones, R. K. W. Spencer, M. W. Matsen and R. H. Grubbs, Manipulating the ABCs of self-assembly via low- $\chi$  block polymer design, *Proc. Natl. Acad. Sci. U. S. A.*, 2017, **114**, 6462.
- 30 D. F. Sunday, A. B. Chang, C. D. Liman, E. Gann, D. M. Delongchamp, L. Thomsen, M. W. Matsen, R. H. Grubbs and C. L. Soles, Self-Assembly of ABC Bottlebrush Triblock Terpolymers with Evidence for Looped Backbone Conformations, *Macromolecules*, 2018, **51**, 7178.
- 31 J. Bolton and J. Rzaev, Synthesis and Melt Self-Assembly of PS-PMMA-PLA Triblock Bottlebrush Copolymers, *Macromolecules*, 2014, **47**, 2864.
- 32 R. Fenyves, M. Schmutz, I. J. Horner, F. V. Bright and J. Rzaev, Aqueous Self-Assembly of Giant Bottlebrush Block Copolymer Surfactants as Shape-Tunable Building Blocks, *J. Am. Chem. Soc.*, 2014, **136**, 7762.
- 33 W. Shen, K. Zhang, J. A. Kornfield and D. A. Tirrell, Tuning the erosion rate of artificial protein hydrogels through control of network topology, *Nat. Mater.*, 2006, **5**, 153.
- 34 Y. Gu, J. Zhao and J. A. Johnson, Polymer Networks: From Plastics and Gels to Porous Frameworks, *Angew. Chem., Int. Ed.*, 2019, DOI: 10.1002/anie.201902900.
- 35 Y. Gu, J. Zhao and J. A. Johnson, A (Macro)Molecular-Level Understanding of Polymer Network Topology, *Trends Chem.*, 2019, **1**, 318.
- 36 M. Zhong, R. Wang, K. Kawamoto, B. D. Olsen and J. A. Johnson, Quantifying the impact of molecular defects on polymer network elasticity, *Science*, 2016, **353**, 1264.
- 37 H. Zhou, J. Woo, A. M. Cok, M. Wang, B. D. Olsen and J. A. Johnson, Counting primary loops in polymer gels, *Proc. Natl. Acad. Sci. U. S. A.*, 2012, **109**, 19119.
- 38 C. Zhou, M. A. Hillmyer and T. P. Lodge, Efficient Formation of Multicompartment Hydrogels by Stepwise Self-Assembly of Thermoresponsive ABC Triblock Terpolymers, *J. Am. Chem. Soc.*, 2012, **134**, 10365.
- 39 C. Zhou, G. E. S. Toombes, M. J. Wasbrough, M. A. Hillmyer and T. P. Lodge, Structure of Two-Compartment Hydrogels from Thermoresponsive ABC Triblock Terpolymers, *Macromolecules*, 2015, **48**, 5934.
- 40 M. K. Gupta, J. R. Martin, B. R. Dollinger, M. E. Hattaway and C. L. Duvall, Thermogelling, ABC Triblock Copolymer Platform for Resorbable Hydrogels with Tunable, Degradation-Mediated Drug Release, *Adv. Funct. Mater.*, 2017, **27**, 1704107.
- 41 M. K. Gupta, J. R. Martin, T. A. Werfel, T. Shen, J. M. Page and C. L. Duvall, Cell Protective, ABC Triblock Polymer-Based Thermoresponsive Hydrogels with ROS-Triggered Degradation and Drug Release, *J. Am. Chem. Soc.*, 2014, **136**, 14896.
- 42 M. Vatankhah-Varnosfaderani, A. N. Keith, Y. Cong, H. Liang, M. Rosenthal, M. Sztucki, C. Clair, S. Magonov, D. A. Ivanov, A. V. Dobrynin and S. S. Sheiko, Chameleon-like elastomers with molecularly encoded strain-adaptive stiffening and coloration, *Science*, 2018, **359**, 1509.
- 43 A. Marabelle, H. Kohrt, C. Caux and R. Levy, Intratumoral Immunization: A New Paradigm for Cancer Therapy, *Clin. Cancer Res.*, 2014, **20**, 1747.

- 44 J. Ishihara, K. Fukunaga, A. Ishihara, H. M. Larsson, L. Potin, P. Hosseinchi, G. Galliverti, M. A. Swartz and J. A. Hubbell, Matrix-binding checkpoint immunotherapies enhance antitumor efficacy and reduce adverse events, *Sci. Transl. Med.*, 2017, **9**, eaan0401.
- 45 N. Momin, N. K. Mehta, N. R. Bennett, L. Ma, J. R. Palmeri, M. M. Chinn, E. A. Lutz, B. Kang, D. J. Irvine, S. Spranger and K. D. Wittrup, Anchoring of intratumorally administered cytokines to collagen safely potentiates systemic cancer immunotherapy, *Sci. Transl. Med.*, 2019, **11**, eaaw2614.
- 46 A. Fakhari, S. Nugent, J. Elvecrog, J. Vasilakos, M. Corcoran, A. Tilahun, K. Siebenaler, J. Sun, J. A. Subramony and A. Schwarz, Thermosensitive Gel-Based Formulation for Intratumoral Delivery of Toll-Like Receptor 7/8 Dual Agonist, MEDI9197, *J. Pharm. Sci.*, 2017, **106**, 2037.
- 47 S. Agrawal and E. R. Kandimalla, Intratumoural immunotherapy: activation of nucleic acid sensing pattern recognition receptors, *Immuno-Oncology Technology*, 2019, **3**, 15.
- 48 D. Christian, R. Philippe, B. Nathalie, C. Alain and C. Bruno, Phase 2 Study of Intratumoral Cisplatin and Epinephrine Treatment for Locally Recurrent Head and Neck Tumors, *Ann. Otol., Rhinol., Laryngol.*, 2004, **113**, 229.
- 49 B. R. Sveinbjörnsson, R. A. Weitekamp, G. M. Miyake, Y. Xia, H. A. Atwater and R. H. Grubbs, Rapid self-assembly of brush block copolymers to photonic crystals, *Proc. Natl. Acad. Sci. U. S. A.*, 2012, **109**, 14332.
- 50 J. Liu, A. O. Burts, Y. Li, A. V. Zhukhovitskiy, M. F. Ottaviani, N. J. Turro and J. A. Johnson, "Brush-First" Method for the Parallel Synthesis of Photocleavable, Nitroxide-Labeled Poly(ethylene glycol) Star Polymers, *J. Am. Chem. Soc.*, 2012, **134**, 16337.
- 51 M. R. Golder, J. Liu, J. N. Andersen, M. V. Shipitsin, F. Vohidov, H. V. T. Nguyen, D. C. Ehrlich, S. J. Huh, B. Vangamudi, K. D. Economides, A. M. Neenan, J. C. Ackley, J. Baddour, S. Paramasivan, S. W. Brady, E. J. Held, L. A. Reiter, J. K. Saucier-Sawyer, P. W. Kopesky, D. E. Chickering, P. Blume-Jensen and J. A. Johnson, Reduction of liver fibrosis by rationally designed macromolecular telmisartan prodrugs, *Nat. Biomed. Eng.*, 2018, **2**, 822.
- 52 P. Shieh, H. V. T. Nguyen and J. A. Johnson, Tailored silyl ether monomers enable backbone-degradable polynorbornene-based linear, bottlebrush and star copolymers through ROMP, *Nat. Chem.*, 2019, **11**, 1124.
- 53 D. Fischer, Y. Li, B. Ahlemeyer, J. Krieglstein and T. Kissel, In vitro cytotoxicity testing of polycations: influence of polymer structure on cell viability and hemolysis, *Biomaterials*, 2003, **24**, 1121.
- 54 A. M. McDonnell, W. J. Lesterhuis, A. Khong, A. K. Nowak, R. A. Lake, A. J. Currie and B. W. S. Robinson, Tumor-infiltrating dendritic cells exhibit defective cross-presentation of tumor antigens, but is reversed by chemotherapy, *Eur. J. Immunol.*, 2015, **45**, 49.
- 55 A. Soeda, Y. Morita-Hoshi, H. Makiyama, C. Morizane, H. Ueno, M. Ikeda, T. Okusaka, S. Yamagata, N. Takahashi, I. Hyodo, Y. Takae and Y. Heike, Regular Dose of Gemcitabine Induces an Increase in CD14<sup>+</sup> Monocytes and CD11c<sup>+</sup> Dendritic Cells in Patients with Advanced Pancreatic Cancer, *Jpn. J. Clin. Oncol.*, 2009, **39**, 797.
- 56 D. R. Green, T. Ferguson, L. Zitvogel and G. Kroemer, Immunogenic and tolerogenic cell death, *Nat. Rev. Immunol.*, 2009, **9**, 353.
- 57 L. W. Pfannenstiel, S. S. K. Lam, L. A. Emens, E. M. Jaffee and T. D. Armstrong, Paclitaxel enhances early dendritic cell maturation and function through TLR4 signaling in mice, *Cell. Immunol.*, 2010, **263**, 79.
- 58 W. M. Liu, D. W. Fowler, P. Smith and A. G. Dalgleish, Pre-treatment with chemotherapy can enhance the antigenicity and immunogenicity of tumours by promoting adaptive immune responses, *Br. J. Cancer*, 2009, **102**, 115.
- 59 A. Sevko, T. Michels, M. Vrohings, L. Umansky, P. Beckhove, M. Kato, G. V. Shurin, M. R. Shurin and V. Umansky, Antitumor Effect of Paclitaxel Is Mediated by Inhibition of Myeloid-Derived Suppressor Cells and Chronic Inflammation in the Spontaneous Melanoma Model, *J. Immunol.*, 2013, **190**, 2464.
- 60 A. Sawant, C. C. Schafer, T. H. Jin, J. Zmijewski, H. M. Tse, J. Roth, Z. Sun, G. P. Siegal, V. J. Thannickal, S. C. Grant, S. Ponnazhagan and J. S. Deshane, Enhancement of Antitumor Immunity in Lung Cancer by Targeting Myeloid-Derived Suppressor Cell Pathways, *Cancer Res.*, 2013, **73**, 6609.
- 61 R. A. Lake and B. W. S. Robinson, Immunotherapy and chemotherapy — a practical partnership, *Nat. Rev. Cancer*, 2005, **5**, 397.
- 62 K. M. Morrissey, T. M. Yuraszeck, C. C. Li, Y. Zhang and S. Kasichayanula, Immunotherapy and Novel Combinations in Oncology: Current Landscape, Challenges, and Opportunities, *Clin. Transl. Sci.*, 2016, **9**, 89.
- 63 L. Zitvogel, L. Apetoh, F. Ghiringhelli and G. Kroemer, Immunological aspects of cancer chemotherapy, *Nat. Rev. Immunol.*, 2008, **8**, 59.
- 64 M. A. Geller, S. Cooley, P. A. Argenta, L. S. Downs, L. F. Carson, P. L. Judson, R. Ghebre, B. Weigel, A. Panoskaltis-Mortari, J. Curtsinger and J. S. Miller, Toll-like receptor-7 agonist administered subcutaneously in a prolonged dosing schedule in heavily pretreated recurrent breast, ovarian, and cervix cancers, *Cancer Immunol. Immunother.*, 2010, **59**, 1877.
- 65 R. Dummer, A. Hauschild, J. C. Becker, J.-J. Grob, D. Schadendorf, V. Tebbs, J. Skalsky, K. C. Kaehler, S. Moosbauer, R. Clark, T.-C. Meng and M. Urosevic, An Exploratory Study of Systemic Administration of the Toll-like Receptor-7 Agonist 852A in Patients with Refractory Metastatic Melanoma, *Clin. Cancer Res.*, 2008, **14**, 856.
- 66 C. G. Park, C. A. Hartl, D. Schmid, E. M. Carmona, H.-J. Kim and M. S. Goldberg, Extended release of perioperative immunotherapy prevents tumor recurrence and eliminates metastases, *Sci. Transl. Med.*, 2018, **10**.
- 67 L. Milling, Y. Zhang and D. J. Irvine, Delivering safer immunotherapies for cancer, *Adv. Drug Delivery Rev.*, 2017, **114**, 79.
- 68 T. Stylianopoulos, L. L. Munn and R. K. Jain, Reengineering the Physical Microenvironment of Tumors to Improve Drug

- Delivery and Efficacy: From Mathematical Modeling to Bench to Bedside, *Trends Cancer*, 2018, **4**, 292.
- 69 B. Andrea, E. J. J. David and A. K. John, Toll-Like Receptor (TLR) Response Tolerance: A Key Physiological “ Damage Limitation ” Effect and an Important Potential Opportunity for Therapy, *Curr. Med. Chem.*, 2006, **13**, 2487.
- 70 C. Bourquin, C. Hotz, D. Noerenberg, A. Voelkl, S. Heidegger, L. C. Roetzer, B. Storch, N. Sandholzer, C. Wurzenberger, D. Anz and S. Endres, Systemic Cancer Therapy with a Small Molecule Agonist of Toll-like Receptor 7 Can Be Improved by Circumventing TLR Tolerance, *Cancer Res.*, 2011, **71**, 5123.
- 71 T. Hayashi, C. S. Gray, M. Chan, R. I. Tawatao, L. Ronacher, M. A. McGargill, S. K. Datta, D. A. Carson and M. Corr, Prevention of autoimmune disease by induction of tolerance to Toll-like receptor 7, *Proc. Natl. Acad. Sci. U. S. A.*, 2009, **106**, 2764.
- 72 S. Gupta, J. Grilley-Olson, D. Hong, A. Marabelle, P. Munster, R. Aggarwal, S. Aspeslagh, R. G. Dixon, M. Patel, V. Subbiah, C. Morehouse, Y. Wu, J. Zha, L. Tseng, Z. A. Cooper, S. Morris and J. Brody, Abstract CT091: Safety and pharmacodynamic activity of MEDI9197, a TLR 7/8 agonist, administered intratumorally in subjects with solid tumors, *Cancer Res.*, 2017, **77**, CT091.
- 73 A. Diab, M. Marcondes, B. Kotzin, M. A. Tagliaferri, U. Hoch, Y. Li, F. Cattaruzza, J. Zalevsky, A. S. Brohl, J. Brugarolas, M. A. Bilen, S. Gupta, E. D. Musibay, A. P. Conley, E. H. Borazanci, S. P. D'Angelo and B. D. Curti, Phase Ib: Preliminary clinical activity and immune activation for NKTR-262 [TLR 7/8 agonist] plus NKTR-214 [CD122-biased agonist] in patients (pts) with locally advanced or metastatic solid tumors (REVEAL Phase Ib/II Trial), *J. Clin. Oncol.*, 2019, **37**, 26.
- 74 J. A. Deane, G. A. Cortez, C. Li, N. Eifler, S. Kasibhatla, N. Parikh, S. Pan and S. Bender, Abstract 4128: Identification and characterization of LHC165, a TLR7 agonist designed for localized intratumoral therapies, *Cancer Res.*, 2019, **79**, 4128.
- 75 S. Stier, C. Maletzki, U. Klier and M. Linnebacher, Combinations of TLR Ligands: A Promising Approach in Cancer Immunotherapy, *Clin. Dev. Immunol.*, 2013, **2013**, 14.
- 76 A. M. Rothschilds and K. D. Wittrup, What, Why, Where, and When: Bringing Timing to Immuno-Oncology, *Trends Immunol.*, 2019, **40**, 12.
- 77 N. Korman, R. Moy, M. Ling, R. Matheson, S. Smith, S. McKane and J. H. Lee, Dosing With 5% Imiquimod Cream 3 Times per Week for the Treatment of Actinic Keratosis: Results of Two Phase 3, Randomized, Double-blind, Parallel-Group, Vehicle-Controlled Trials, *Arch. Dermatol.*, 2005, **141**, 467.
- 78 K. Peris, E. Campione, T. Micantonio, G. C. Marulli, M. C. Fagnoli and S. Chimenti, Imiquimod Treatment of Superficial and Nodular Basal Cell Carcinoma: 12-Week Open-Label Trial, *Dermatol. Surg.*, 2005, **31**, 318.
- 79 G. Chen and L. A. Emens, Chemoimmunotherapy: reengineering tumor immunity, *Cancer Immunol. Immunother.*, 2013, **62**, 203.
- 80 A. Tzeng, M. J. Kauke, E. F. Zhu, K. D. Moynihan, C. F. Opel, N. J. Yang, N. Mehta, R. L. Kelly, G. L. Szeto, W. W. Overwijk, D. J. Irvine and K. D. Wittrup, Temporally Programmed CD8 $\alpha$ + DC Activation Enhances Combination Cancer Immunotherapy, *Cell Rep.*, 2016, **17**, 2503.
- 81 Y. Jiang, Y. Li and B. Zhu, T-cell exhaustion in the tumor microenvironment, *Cell Death Dis.*, 2015, **6**, e1792.